RESEARCH ARTICLE

Island Arc WILEY

A Paleogene magmatic overprint on Cretaceous seamounts of the western Pacific

Naoto Hirano[1,2] | Hirochika Sumino[3] | Taisei Morishita[4] |
Shiki Machida[5] | Takaomi Kawano[2] | Kazutaka Yasukawa[6,5] |
Takafumi Hirata[7] | Yasuhiro Kato[6,5] | Teruaki Ishii[8]

[1]Center for Northeast Asian Studies, Tohoku University, Sendai, Japan

[2]Graduate School of Science, Tohoku University, Sendai, Japan

[3]Graduate School of Arts and Sciences, The University of Tokyo, Tokyo, Japan

[4]Hydrographic and Oceanographic Department, Japan Coast Guard, Tokyo, Japan

[5]Ocean Resources Research Center for Next Generation, Chiba Institution of Technology, Chiba, Japan

[6]School of Engineering, The University of Tokyo, Tokyo, Japan

[7]Geochemical Research Center, The University of Tokyo, Tokyo, Japan

[8]Center for Integrated Research and Education of natural Hazards, Shizuoka University, Shizuoka, Japan

Correspondence
Naoto Hirano, Center for Northeast Asian Studies, Tohoku University, 41 Kawauchi, Aoba-ku, Sendai 980–8576, Japan.
Email: nhirano@tohoku.ac.jp

Abstract

The West Pacific Seamount Province (WPSP) represents a series of short-lived Cretaceous hotspot tracks. However, no intraplate volcanoes in advance of petit-spot volcanism erupted near a trench have been identified after the formation of the WPSP on the western Pacific Plate. This study reports new ages for Paleogene volcanic edifices within the northern WPSP, specifically the Ogasawara Plateau and related ridges, and Minamitorishima Island. These Paleogene ages are the first reported for basaltic rocks on western Pacific seamounts, in an area that has previously only yielded Cretaceous ages. The newly found Paleogene volcanisms overprint the Early–middle Cretaceous volcanic edifices, because the seamount or paleo-island material-covered reefal limestone caps on these edifices are uniformly older than the Paleogene volcanism identified in this study. This study outlines several possible causative factors for the Paleogene volcanism overprinting onto existing Cretaceous seamounts, including volcanism related to lithospheric stress, or a younger hotspot track within the northern part of the WPSP that records magmatism from ∼60 Ma.

KEYWORDS
alkali-basalt, hotspot, Pacific plate, Paleogene, petit-spot, rejuvenation, seamount

1 | INTRODUCTION

Significant eustatic sea level and global average temperature changes occurred during the mid-Cretaceous, along with increased seafloor spreading rates and voluminous volcanism (Hardebeck & Anderson, 1996; Larson, 1991). The majority of the seamounts in the western Pacific Plate also formed at this time, but were instantaneously submerged as a result of a contemporaneous eustatic sea level rise (Figure 1). Koppers et al. (2003) assigned all seamounts older than 70 Ma in this area to the West Pacific Seamount Province (WPSP), and determined that the seamount distribution within the province details short-lived hotspot trails that formed within the present-day French Polynesian hotspots of the South Pacific. However, some of the seamount chains within the province cannot be explained using a
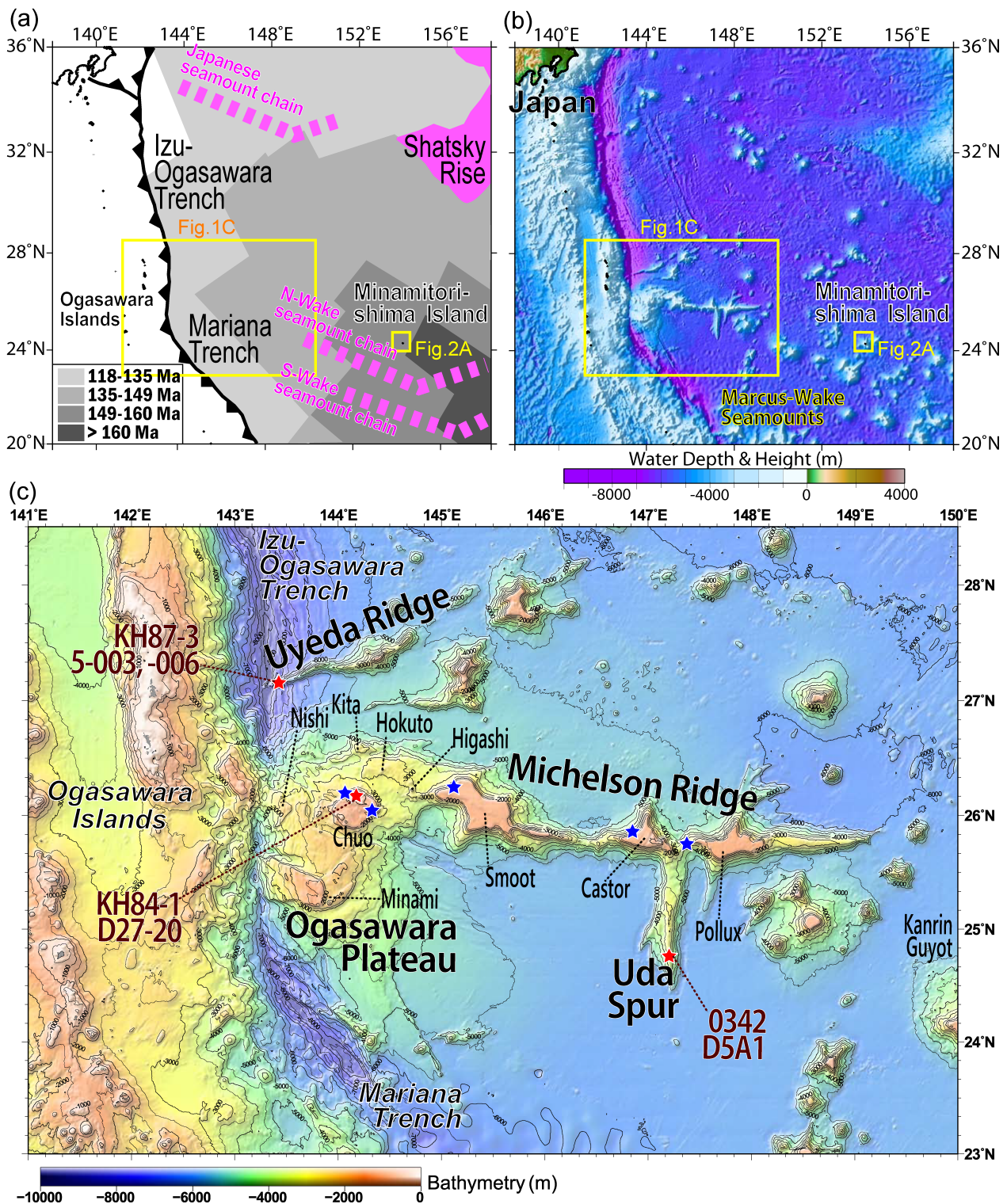
FIGURE 1 Tectonic and bathymetric maps of the study area. The two small figures (a) and (b) show respectively the seafloor ages and seamount chains in the area of northern part of Western Pacific Seamount Province (WPSP), and bathymetric map of the western Pacific Plate. (c) Bathymetrc map around the Ogasawara Plateau and related ridges that form the focus of this study (Ohara et al., 2015). Red stars indicate sampling sites from this study; blue stars show the sites reported reefal limestones dated during previous studies (Konishi, 1985; Shiba, 1989; Takayanagi et al., 2007)

classical hotspot hypothesis, such as that outlined for the Hawaii–Emperor seamount chain. The seamount chains do not exhibit linear age progression, which could be explained by (1) the overlap of a

hotspot track with a younger hotspot (e.g., the Magellan seamount chain: Koppers et al., 1998), (2) coeval volcanism along pre-existing lithospheric fractures like what has been suggested for the Line

Islands (Davis et al., 2002), or (3) the presence of recycled material within the upper mantle immediately after a continental breakup event (some examples of Indian ocean volcanism; Taneja et al., 2016).

It is theoretically difficult to identify the timing of seamount formation using a single radiometric age. This is exemplified by the present-day Hawaiian shield volcano, which records a few million years of seamount edifice evolution (Macdonald & Katsura, 1964). Recent research on the Aitutaki Island along the Cook–Austral hotspot track identified a rejuvenated stage of volcanism some 7–8 million years younger than the main shield stage volcanoes and the older volcanism on Aitutaki Island (Jackson et al., 2020). Geochronological research on Cretaceous seamounts has also determined that longer-lived main shield stages of volcanism are significantly longer than the timespan of present-day oceanic island volcanism on the Pacific Plate. Hirano et al. (2002) determined that a single seamount may have a long-lived evolution of at least 10 my by investigating the ages of main (hawaiite) and late (differentiated) shield lavas. It is possible that Cretaceous seamounts within the Pacific Plate have remained stationary above hotspots for longer than would normally be the case because of the slower absolute motion of the plate during the Early Cretaceous (3–6 cm/year; Henderson et al., 1984; Duncan & Clague, 1985). This is also the case for the present-day Canary and Cape Verde hotspots, and the associated slow absolute motion of the northern African Plate (Geldmacher et al., 2001).

Numerous seamounts and knolls have left evidence of volcanic activity within the western Pacific Plate. This includes the recently described lithospheric flexure-induced volcanoes (i.e., petit-spots) in the outer rises of the Japan and Mariana trenches prior to the subduction of the northwestern and western margins of the Pacific Plate (Hirano et al., 2006, 2019). However, no petit-spot volcanic activities preceding intraplate volcanism have been identified within the younger Late Cretaceous WPSP hotspots of the western Pacific Plate. This study presents new geochronological data for island, seamount, plateau, ridge, and spur samples from the WPSP, and uses these data to outline the evolution of hotspot volcanism within the western Pacific Plate.

2 | GEOLOGIC SETTINGS

The western Pacific Plate, hosting numerous seamounts, formed at ~180–140 Ma (Handschumacher et al., 1988; Figure 1a,b). As mentioned above, Koppers et al. (2003) delineated the Early–Late Cretaceous WPSP. These seamounts are thought to have formed from secondary plumelets derived from the top of the South Pacific superplume, similar to the present-day hotspot magmatism in French Polynesia (Koppers et al., 2003). The short-lived southern Marcus–Wake seamounts (Sager et al., 1993; Southern Wake seamount chain of Koppers et al., 2003) formed at 120–100 Ma. The age progression within the northern section of the Marcus–Wake seamounts around Marcus Island (Northern Wake seamount chain of Koppers et al., 2003) has also been determined through whole-rock Ar–Ar dating of two seamounts (113 and 101 Ma: Winterer et al., 1993; Koppers et al., 2003). Minamitorishima Island and the Ogasawara Plateau are located respectively 100–200 km north and 500 km west of the mid-Cretaceous (~100 Ma) hotspot track of the Northern Wake seamount trail (Figure 1a,b). Minamitorishima Island is an emerged table reef that developed on the summit region of a volcanic edifice. This island is unique within the northern WPSP, as the next closest island, Wake Island, is ~1300 km to the southeast.

The Ogasawara Plateau and Michelson Ridge are adjacent to the ESE–WNW trending Marcus–Wake seamounts. The western part of the plateau is currently being subducted at the Izu–Ogasawara and Mariana trenches, and/or is colliding with the Izu-Ogasawara and Mariana Arcs, dividing this trench–arc system topographically and systematically between the Izu–Ogasawara and Mariana trenches. The geomorphological features of the Ogasawara Plateau record the amalgamation of several edifices. These include the Higashi and Chuo seamounts, the Nishi, Hokuto, and Minami hills, and the Kita knoll, some of which are thought to represent individual seamounts that have been forced into a trench, which has been determined through detailed bathymetric and structural interpretation (Smoot, 1983; Nagaoka et al., 1989; Figure 1c). The 500 km long, 95°–275°-trending Michelson Ridge is connected to the Ogasawara Plateau, and is associated with the Smoot, Caster, and Pollux guyots (Figure 1c). The Uda Spur is the largest spur in this area, and trends southwards away from the ridge (Figure 1c).

The Uyeda Ridge lies ~80 km north of the Ogasawara Plateau, and is currently being subducted into the Izu–Ogasawara Trench, forming an oceanward-trending slope at the westernmost part. Smoot and Heffner (1986) speculated that this ridge represents either an extinct spreading center or a location where magma has leaked along a tectonic structure, as the ridge is topographically elongated NNW–SSW, parallel to the paleomagnetic lineations present in the seafloor in this area.

2.1 | Geochronological studies

The presence of a distinctive magnetic anomaly along the Ogasawara Plateau and Michelson Ridge occludes the magnetic lineations within the surrounding seafloor, indicating that these areas represent areas of intraplate volcanism that occurred after formation of the surrounding oceanic crust at a mid-ocean ridge (Kasuga et al., 1995). The thickness of the reefal limestones that cover the Ogasawara Plateau and Michelson Ridge areas varies from thicker reefs in the Minami Hill area (the westernmost part of the plateau and ridge), to thinner reefs in the Pollux Guyot area (easternmost plateau and ridge). This suggests that the seamounts in this area have subsided in a direction parallel to the paleo-plate motion recorded in this area (Okamura et al., 1992).

Reefal limestones from the Chuo Seamount of the Ogasawara Plateau yield Albian to Cenomanian (112–93.5 Ma) microfossil ages (Konishi, 1985). Foraminiferas from the Smoot Guyot record the presence of coral reefs before the mid-Cretaceous rise in sea level between the Cenomanian and Turonian (100–90 Ma), corresponding with the ages of fossils within apatite-altered limestones in this area (Shiba, 1979). Reefal carbonates in this region have yielded Sr isotopic ages of 83.3 Ma (Smoot Guyot), 85.7 Ma (Castor Guyot), and 84.0 Ma (Pollux Guyot) (Takayanagi et al., 2007) (Figure 1c). Although the Uda

TABLE 1   Sampling sites and rock descriptions

Location	Geography	Cruise#	Sample#	Site		Sampling	Description		
				Latitude	Longitude		Rock	Phenocryst	Groundmass
Uyeda Ridge	Western tip of the ridge	R/V Hakuho, KH87-3	D5-003	27 08.3″N	143 26.7″E	Dredge	Olivine basalt	Ol (pseudomorph)	Pl, CrSp, Altered minerals
	Western tip of the ridge	R/V Hakuho, KH87-3	D5-006	27 08.3″N	143 26.7″E	Dredge	Olivine basalt	Ol (pseudomorph)	Pl, CrSp, Altered minerals
Ogasawara Plateau	Knoll on the Chuo Seamount	R/V Hakuho, KH84-1	D27-20	26 11.6′N	144 10.5′E	Dredge	Vesicular, olivine basalt	Ol (pseudomorph)	Pl, Altered minerals
Uda Spur	Ridge crest	S/V Takuyo, 0342	D5A1	24 45.4″N	147 12.3″E	Dredge	Olivine basalt, quenched glass rind	Ol (fresh)	Pl, Cryptocrystalline
Minamitorishima Island	Terrace, NW slope of the island's edifice	Shinkai6500, 6K1209	R02	24 21.2415′N	153 53.0887″E	Submersible	Olivine basalt	Ol (fresh)	Cpx, Cryptocrystalline
	Terrace, NW slope of the island's edifice	Shinkai6500, 6K1209	R03	24 21.2415′N	153 53.0887″E	Submersible	Olivine basalt	Ol (fresh)	Cpx, Cryptocrystalline
	Knoll, NW slope of the island's edifice	Shinkai6500, 6K1209	R10	24 20.4198′N	153 53.2929″E	Submersible	Highly vesicular, olivine basalt	Ol (partly fresh)	Cryptocrystalline
	Knoll, NW slope of the island's edifice	Shinkai6500, 6K1209	R14	24 20.3859′N	153 53.3232″E	Submersible	Highly vesicular, basalt	aphyric	Cryptocrystalline
	Below ridge, NW slope of the island's edifice	Shinkai6500, 6K1209	R18	24 19.6913′N	153 52.7729″E	Submersible	Vesicular, olivine basalt	Ol (pseudomorph)	Cpx, Altered minerals, Cryptocrystalline
	Below ridge, NW slope of the island's edifice	Shinkai6500, 6K1209	R19	24 19.5953′N	153 52.7808″E	Submersible	Vesicular, olivine basalt	Ol (pseudomorph)	Altered minerals, Cryptocrystalline

Abbreviations: CrSp, chromian spinel; Cpx, clinopyroxene; Ol, olivine; Pl, plagioclase.

Spur, Uyeda Ridge, and Minamitorishima Island areas have not been dated, Aftabuzzaman et al. (2021) report late Early Cretaceous ages for reefal limestones obtained from a submarine slope of the island's edifice.

3 | ROCK SAMPLINGS AND METHODS

Basaltic rock samples were obtained during dredging of four volcanic edifices within the WPSP, namely the Chuo Seamount on the Ogasawara Plateau (sample KH84-1 D27-20), the Uyeda Ridge (KH87-3 5-003 and -006), and the Uda Spur (0324 D5A1) (Table 1; Figure 1c); samples were retrieved during cruises KH84-1 and KH87-3 of *R/V HAKUHO-MARU* and cruise #0324 of *R/V TAKUYO*. The KH84-1 D27-20 sample was obtained from a small knoll (600 to 800 m depth) on the Chuo Seamount (a guyot) of the Ogasawara Plateau. The knoll is a few km in diameter, is around 100–200 meters tall, and is located on the 40 km diameter, flat-topped Chuo Seamount at a water depth of −900 to −1300 m (Konishi, 1985). Samples KH87-3 5-003 and -006 were obtained from a fault escarpment with associated horst and graben structures on the oceanward slope of a trench at a depth of −6000 m. These structures reflect the subduction of the eastern tip of the east to west oriented Uyeda Ridge into the Izu–Ogasawara Trench. Finally, sample 0324 D5A1 was dredged from the southern part of a ridge crest along the Uda Spur (Table 1; Figure 1c).

A dive was undertaken during the cruise of YK10-05 of *R/V YOKOSUKA*, using the submersible *Shinkai6500* along the northwestern submarine slope of the Minamitorishima Island (Figure 2a). Basaltic rock samples were obtained during this dive into the northwestern flank of the volcanic edifice associated with several topographic ridges and cones. Observations during this dive identified topographic structures that likely reflect lava flows (6K1209-R02, -R03), volcanic cones (6K1209-R10, -R14), and volcanic ridges (6K1209-R18, -R19), with the resulting samples termed terrace, knoll, and ridge samples, respectively, in this study (Table 1; Figure 2b).

3.1 | Petrography and geochemistry

Samples from the Chuo Seamount on the Ogasawara Plateau (KH84-1 D27-20), the Uyeda Ridge (KH87-3 5-003, -006), and the knoll and ridge sites of submarine slope of the Minamitorishima Island (6K1209 R10, -R14, -R18, -R19) are all basalt, partly vesicular and altered, with a groundmass containing plagioclase or clinopyroxene (Table 1; Figure 3). Samples KH87-3 5-003, -006, and 0324 D5A1 also contain chromian spinel located around olivine phenocryst pseudomorphs or fresh olivines. The single basaltic sample from the Uda Spur (0324 D5A1) has a fresh glass rind and phenocrystic olivines (Table 1). Finally, the samples from the terrace site of submarine slope of the Minamitorishima Island are fresh, dense, olivine-bearing basalts in opposition to highly vesicular and altered basalt from the ridge and knoll sites (Table 1; Figure 3). Prior to analysis, the small sections of each sample were soaked in pure water for more than 24 h to remove any seawater contamination.
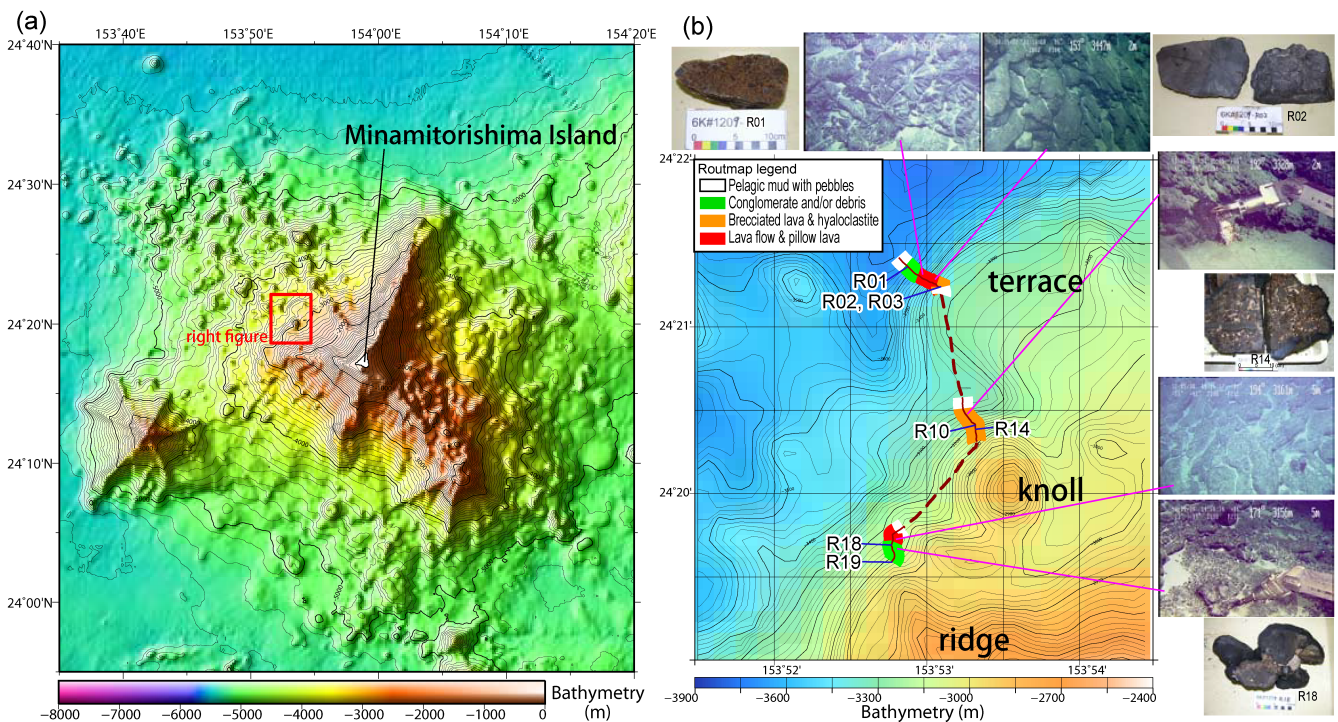
FIGURE 2 The map gives the detailed bathymetry around Minamitorishima Island (a) (Oikawa & Morishita, 2009), and the observations along a submersible dive track along the northwestern slope of the island's edifice (b). The seven sampling sites from this study are labelled as R01–R19, with the photographs of representative observations and rocks obtained by the submersible *SHINKAI6500* shown as insets. The map (b) has a 20 m contours, and it was obtained using the shipboard SeaBeam2112 system during the YK10-05 cruise (available at the DARWIN website: http://www.godac.jamstec.go.jp/darwin/e)

FIGURE 3 Photomicrograph of age-determined samples. (a) 0342 D5A1, (b) KH84-1 D27-20, (c) KH87-3 D5-006, (d) 6K1209 R02, (e) 6K1209 R10, and (f) 6K1209 R18

The bulk rock geochemical compositions were determined using a X-ray fluorescence spectrometer. Major elements were analyzed with glass beads (1 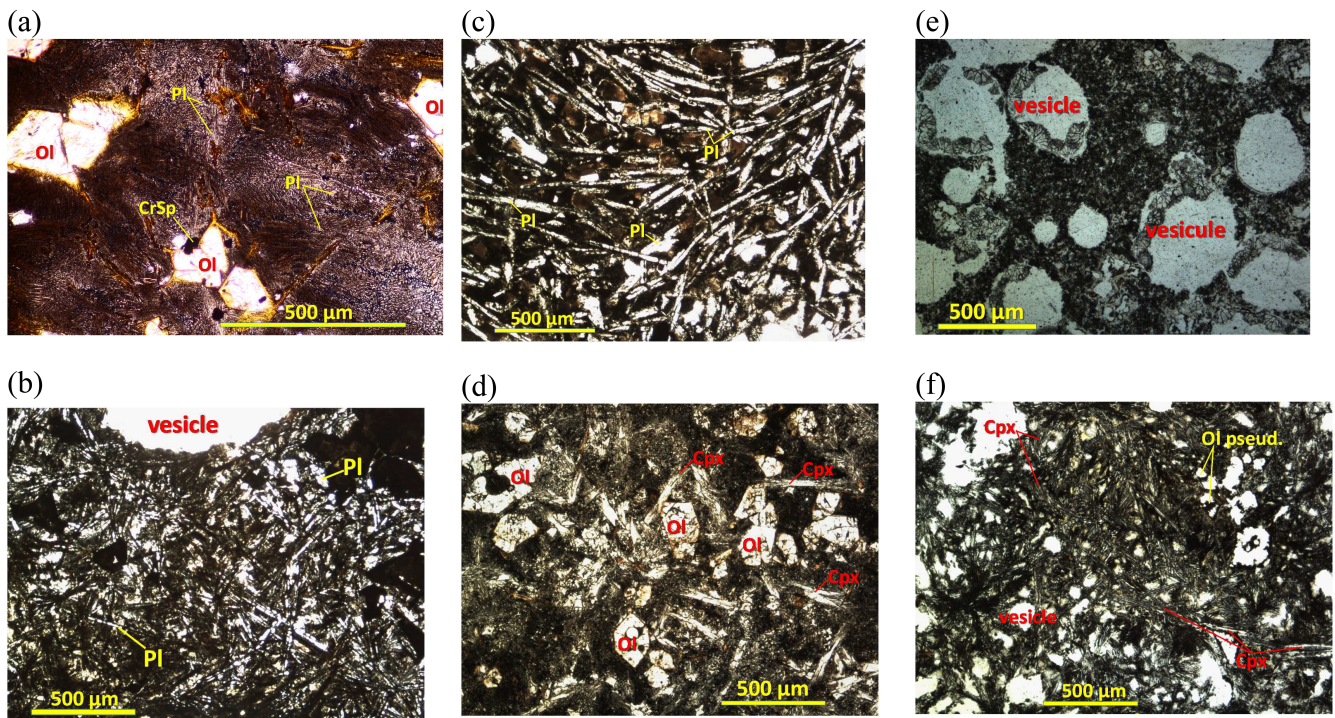g sample to 5 g lithium tetraborate) by a Rigaku RIX2000 at the Department of Earth Sciences, Tohoku University. Bulk rock trace element compositions were determined using an Agilent 7500c quadrupole inductively coupled plasma–mass spectrometry (ICP–MS) at the School of Engineering, the University of Tokyo. Samples were prepared following Kato et al. (2005, 2011) and Machida et al. (2008, 2015). A total of 0.05 g of powdered rock sample was completely dissolved in 0.8 ml $HClO_4$, 4.0 ml HF, and 2.0 ml HNO_3, in a tightly sealed 10 ml Teflon PFA screw-cap beaker. The solution was heated for 2 h at 130 °C before being progressively evaporated for more than 12 h at 110 °C, for 6 h at 160 °C, and finally at 180 °C until full evaporation. The residue was then re-dissolved in a 1 ml HNO_3–HCl–HF (20:5:1) mixed acid solution by heating for 20 min at 80 °C before being further heated for 2 h at 110 °C after adding 4 ml of 18.3 MΩ*cm water. The resulting solution was diluted to a mass ratio of 1:2000 using 18.3 MΩ*cm water. We also analyzed a reference basalt (JB-2: Imai et al., 1995), yielding results that were typically within 5 % (relative standard deviation) of the certified composition.

The chromian spinels in the samples, KH87-3 5-003 and -006 (Uyeda Ridge) are analyzed by a JEOL JXA-733 electron microprobe analyzer at the former Ocean Research Institute (present Atmosphere and Ocean Research Institute), University of Tokyo, with 15 kV accelerating voltage and 12 nA probe current using focused beam.

The quenched glass rind of the sample, 0324-D5A1 (Uda Spur), was analyzed by electron microprobe analysis for major elements and

laser ablation ICP-MS for trace elements. The major elements were analyzed by JEOL JXA-8800 at the Tokyo Institute of Technology. Although analyzing conditions were the same as those for KH87-3 5-003 and -006, we utilized unfocused beam with a diameter of ~10 μm. Data were averaged in 5 points. Trace element compositions were analyzed by quadrupole ICP-MS using laser ablation methods. VG PlasmaQuad 2 was connected to the 193-nm ArF Excimer laser ablation system (GeoLas 200 CQ). Analysis was operated using argon and helium mixing nebulization, following procedures described elsewhere (Norman et al., 1998). The internal standardization used Ca contents determined by electron microprobe. For quantitative analysis, the ablation (5 Hz) was performed on at least five spots (32 μm in diameter) and calibrated using the NIST612 glass as the standard. The resulting precision, as checked by a standard reference material (analyzed as an unknown), was better than 10 % (2 std. dev.) for most elements.

3.2 | Ar-Ar datings

For the $^{40}Ar/^{39}Ar$ dating, the separated groundmass phases from all basaltic samples were crushed to 100–300 μm grains except for the sample KH87-3 5-006 prepared as a few millimeter-sized small tip due to their limited size of the rock. All samples were leached by HNO_3 (1 mol/L) for 1 h in order to remove clays and altered materials except for the tip sample of KH87-3 5-006. All samples were finally washed in ultrasonic pure water and acetone.

The samples were wrapped in aluminum foil with K_2SO_4, CaF_2 and flux monitors which are HD-B1 and Bern4B (Flish, 1982; Hess &

Lippolt, 1994) for the samples of KH87-3 5-006, and JG-1 biotite (Iwata, 1998) for all other samples. The samples of 0324D5A1, KH84-1 D27-20, and KH87-3 5-006) were irradiated for 24 h in the Japan Material Testing Reactor (JMTR), Tohoku University. During the irradiation, samples were shielded by Cd foil in order to reduce neutron-induced ^{40}Ar from ^{40}K. The samples of 6K1209-R10, -R02, and -R18 were irradiated for 3 h without Cd-foil in the Kyoto University Research Reactor (KUR), Kyoto University. The argon extraction and isotopic analyses were operated at the University of Tokyo for the samples, 0324D5A1, KH84-1 D27-20, and KH87-3 (5-003 and -006). The extraction and analysis for the samples, KH87-3 5-006, were carried out at Yamagata University. During incremental heating the gases were extracted in 8 to 13 steps between 500 °C and 1500 °C.

4 | RESULTS

4.1 | Dive observations of the northwestern slope of Minamitorishima Island

Shipboard multibeam sonar surveys yielded detailed bathymetric images of the volcanic cones and ridges on the seamount slope of Minamitorishima Island (Figure 2a). The submersible dive 6K#1209 was undertaken on the terrace, cone, and ridge areas of the northwestern mid-slope of the island's edifice. The cones in this area are several hundred meters tall and ~1 km in diameter. The lava flows are predominantly located in the terrace area, and are associated with breccias. The knoll site consists of highly vesicular, altered, and brecciated lavas and hyaloclastites, in contrast with the dense lavas at the terrace site (Figure 2b).

A steep cliff marking the lower edge of the terrace consists of truncated pillows and pillow lavas, with a basal section consisting of conglomerates and breccias. Clearly pillow structures are also visible within the cliffs, and are coated with a ferromanganese crust (Figure 2b). The gentle slope above the terrace area is predominantly covered by pelagic sediment. The knoll site contains massive rocks that have botryoidal surfaces that reflect the formation of ferromanganese crusts. Although it was too hard to sample the lobate lavas at the ridge site, debris material and conglomerates containing highly vesicular and altered rocks were sampled at the bottom of the ridge (Figure 2b).

4.2 | Geochemistry

The bulk rock geochemistry of the fresh samples analyzed in this study (sample 0324-D5A1 from the Uda Spur and samples 6K1209-R10, -R14, -R18, and -R19 from the Minamitorishima Island) is similar to that of the pattern of intraplate basalts. Sample 0324-D5A1 is classified as a non-alkali basalt as it contains a higher SiO_2 content than the other samples (~50 wt%, Table 2; Figure 4a). Normative composition discriminates between alkaline basalts for 6K1209-R03, -R03, -R14,

and -R19) and olivine tholeiites for 0324 D5A1, and 6K1209-R18 without normative quartz (Table 2). The bulk rock composition of sample 6K1209-R14 has most likely been influenced by seawater-related alteration, as the total major element content within this sample is lower than the other, fresher samples, and the SiO_2, CaO, and P_2O_5 contents are inconsistent with those generally expected for basaltic rocks (Table 2). The large ion lithophile element (LILE; e.g., Ba, Th, U, Ce, and Sr) contents of this sample also vary significantly as a result of alteration, as evidenced by their multi-element variation diagram patterns (thin brown line in Figure 4b) (Ludden & Thompson, 1978; Philpotts & Hart, 1969). As such, more immobile high field strength elements (HFSEs) are used to discuss the magmatic origins of these samples, including altered sample 6K1209-R14. The chromian spinel-bearing, altered samples analyzed during this study (KH87-3 5-003 and -006) have typical alkaline intraplate basalt compositions (i.e., higher TiO_2 content than those expected for MORB and arc-type basalts; Table 3; Figure 4c).

4.3 | Whole-rock Ar-Ar age datings

The ages of six samples were determined by incremental heating-type $^{40}Ar/^{39}Ar$ age dating during this study, namely samples 0342-D5A1 (Uda Spur) (Figure 5a), KH84-1 D27-20 (a knoll on the Chuo Seamount of the Ogasawara Plateau) (Figure 5b), KH87-3 5-006 (Uyeda Ridge) (Figure 5c), and 6K1209-R02, -R10, and -R18 (from Minamitorishima Island) (Figure 5d–f). The data and analytical conditions are shown in Table S1. Most of these samples yield the step-wise heating patterns in Ar–Ar ratio similar to those obtained for crystalline groundmass separates from altered seamount basalts in the region. These consist of old and young apparent age fractions obtained from heating at lower and higher temperatures, respectively. They are due to the recoil effect for $^{39}Ar_K$ and $^{37}Ar_{Ca}$ during irradiation of sample (Koppers et al., 2000, 2003). As such, the fractions obtained from heating at intermediate temperatures remove these higher and lower temperature effects, and are therefore used to determine the formation ages of the samples in this study.

The sample 6K1209-R18 contains excess Ar that yields initial $^{40}Ar/^{36}Ar$ ratio of 336.3 ± 7.8, meaning the isochron age is the preferred age (Figure 5f). The sample KH87-3 5-006 plausibly yields an excess Ar ($^{40}Ar/^{36}Ar$ = 356 ± 1000) during middle temperatures as well. A plateau age during higher temperatures in the sample of KH87-3 5-006 would be ignored as an apparent age because their ages are obviously younger than those on intermediate temperature fractions (Figure 5c). The sample, 0342-D5A1, accepts the isochron age because of lower $^{40}Ar/^{36}Ar$ intercept in inverse isochron due to mass fractionation probably during lava-quenching or step-wise heating (Figure 5a). The plateau ages of the intermediate temperature fractions of the other three samples are used as their preferred Ar–Ar ages (Figure 5b,d,e). The large uncertainties for each fraction of sample 6K1209-R10 reflect the low $^{39}Ar/^{40}Ar$ ratios obtained from this sample. This reflects lower K contents in the presence of remnant plagioclase within the groundmass separates that remained after

TABLE 2 Geochemical results of major, trace, and normative compositions

Site	Uda Spur	Minamitorishima Island Terrace		Knoll	Ridge	
Sample #	0324-D5A1 Glass	6K1209-R02 Bulk	6K1209-R03 Bulk	6K1209-R14 Bulk	6K1209-R18 Bulk	6K1209-R19 Bulk
Method	Electron[a] microprobe	XRF	XRF	XRF	XRF	XRF
Major elements (wt%)						
SiO_2	48.93	45.94	45.02	37.10	46.56	45.88
TiO_2	2.56	2.10	2.19	2.37	2.18	2.79
Al_2O_3	13.67	13.49	13.75	10.95	15.27	15.17
FeO^b	9.98	13.04	14.64	9.55	12.37	14.14
MnO	0.15	0.17	0.17	0.08	0.12	0.13
MgO	6.53	7.63	8.07	6.50	3.84	3.82
CaO	10.45	9.94	9.97	17.57	10.77	9.90
Na_2O	2.82	0.99	2.72	2.22	1.22	3.51
K_2O	0.44	3.58	0.93	1.99	3.18	1.48
NiO	0.01	—	—	—	—	—
P_2O_5	0.18	0.19	0.20	3.36	0.56	0.60
Cr_2O_3	0.04	—	—	—	—	—
Total	95.74	97.08	97.65	91.68	96.06	97.43
Method	LA-ICPMS[a]	ICPMS	ICPMS	ICPMS	ICPMS	ICPMS
Trace elements (µg/g)						
Rb	9.5	13.8	12.4	28.1	18.8	17.0
Sr	294	377	346	407	584	562
Y	32.0	20.6	19.9	39.2	34.9	38.0
Zr	201	162	153	164	194	186
Nb	23.7	26.8	25.3	36.5	37.3	36.0
In	0.18	—	—	—	—	—
Sn	2.9	—	—	—	—	—
Cs	0.15	0.20	0.18	0.70	0.68	0.57
Ba	89.0	251	224	237	392	371
La	20.2	26.5	25.9	63.4	47.4	47.1
Ce	48.3	52.5	49.4	56.2	70.0	67.0
Pr	6.3	6.4	6.1	10.5	10.8	9.6
Nd	29.8	26.8	25.4	43.6	44.7	39.9
Sm	7.1	6.1	5.6	8.2	9.6	8.3
Eu	2.4	2.1	1.9	2.6	2.9	2.6
Gd	7.2	6.1	5.7	8.3	9.5	8.6
Tb	1.1	0.87	0.83	1.0	1.3	1.2
Dy	6.7	4.9	4.6	5.7	7.4	6.7
Ho	1.2	0.88	0.83	1.1	1.3	1.3
Er	3.3	2.3	2.1	2.9	3.4	3.4
Tm	0.43	0.29	0.27	0.37	0.44	0.44
Yb	3.0	1.8	1.7	2.3	2.6	2.7
Lu	0.38	0.23	0.23	0.33	0.34	0.37
Hf	5.1	4.0	3.7	3.9	4.7	4.6
Ta	1.4	1.9	1.8	3.0	2.6	2.6
W	0.21	—	—	—	—	—
Pb	1.5	2.0	1.9	1.6	7.8	2.7
Th	1.9	3.1	3.0	3.2	3.4	3.3
U	0.54	0.67	0.63	1.6	1.0	1.0

TABLE 2 (Continued)

| Site | Uda Spur | Minamitorishima Island Terrace | | Knoll | Ridge | |
| Sample # | 0324-D5A1 | 6K1209-R02 | 6K1209-R03 | 6K1209-R14 | 6K1209-R18 | 6K1209-R19 |
	Glass	Bulk	Bulk	Bulk	Bulk	Bulk
Normative wt%[c]				[d]		
Quartz						
Plagioclase	47.1	27.8	39.2	14.0	37.0	41.8
Orthoclase	2.5	21.1	5.4		18.8	8.8
Nepheline		1.3	3.5	10.1		4.9
Leucite				9.2		
Diopside	22.3	21.7	21.2	33.0	19.5	20.5
Hypersthene	16.4				6.8	
Olivine	0.4	18.6	21.4	8.1	6.6	12.6
Larnite				3.4		
Ilmenite	4.8	4.0	4.2	4.5	4.1	5.3
Magnetite	1.6	2.1	2.4	1.6	2.0	2.3
Apatite	0.4	0.4	0.5	7.8	1.3	1.4

Note: '–' symbols represent below detection limit.
[a]Average values of five point analysis.
[b]FeO as total values.
[c]Assuming 10 % Fe^{3+} in total iron.
[d]As a reference of highly altered rock.

the altered sample was acid-leached. Some of age results do not provide adequate quality for submarine altered basalts (e.g. the high probability of fit values for the plateau ages of KH84-1 D27-20 and 6K1209-R02, and the age defined by 3-steps for KH84-1 D27-20 and KH87-3 D5-006) (Figure 5). The samples analyzed during this study yield Ar–Ar ages in 2-sigma of 104.3 ± 2.8 (Uda Spur), 55.3 ± 1.2 (knoll on the Chuo Seamount, Ogasawara Plateau), 57.9 ± 1.7 (Uyeda Ridge), and 40.19 ± 0.98, 33.2 ± 3.8, and 37.54 ± 0.70 Ma (all from Minamitorishima Island's edifice) (Figure 5).

5 | DISCUSSION

This study reports the first Paleogene ages for basaltic rocks within the WPSP, an area that has only previously yielded Cretaceous ages. Previously obtained Upper Cretaceous ages for limestones from the Chuo Seamount and the Minamitorishima Island's edifice (Aftabuzzaman et al., 2021; Konishi, 1985; Shiba, 1979) indicate that these areas must have hosted Cretaceous volcanic seamounts prior to the formation of these reefal limestone caps. The Paleogene basalts from the Chuo Seamount and Minamitorishima Island dated in this study are therefore thought to reflect volcanic events that overprinted the Cretaceous volcanic edifices in this region. In addition, the geochronological data for the Uyeda Ridge presented in this study suggest that this feature is not explained by a fossil spreading center, as suggested by Smoot and Heffner (1986).

Some examples of rejuvenated seamounts within the WPSP were identified during Ocean Drilling Program Leg 144. This research determined that ~100 Ma reefal limestones of the Wodejebato Guyot, located in the south of the WPSP and neighbor of the northeast of Bikini Atoll, are covered with the products of a Campanian (80–70 Ma) volcanic event (Ocean Drilling Program Leg 144 Shipboard Scientific Party, 1993). The Early Cretaceous MIT Guyot (Figure 6) also records ~117 Ma shallow marine phreatomagmatic eruptions that penetrated a carbonate platform (Martin et al., 2004). However, no research has yet identified post-Cretaceous rejuvenating volcanic events on pre-existing Cretaceous seamounts within the WPSP.

5.1 | Ogasawara Plateau and related ridges

The whole-rock Ar–Ar age of 104.3 ± 2.8 Ma obtained from a sample from the Uda Spur represents the first possible age of a basement edifice within the Ogasawara Plateau and related ridges (i.e., the Michelson Ridge connecting to the Uda Spur). This is consistent with the clustering of ages for the limestone platforms along the Ogasawara Plateau and Michelson Ridge at 110–80 Ma (Konishi, 1985; Shiba, 1979; Takayanagi et al., 2007). The Late Cretaceous ages of reefal limestone from the Pollux, Castor, and Smoot guyots, as well as potentially the Uda Spur, are certainly consistent with the presence of Cretaceous volcanic edifices in this area. The reefal limestone caps are also thicker in the western plateau, ridges, and guyots within this region, suggesting that the seamounts in this area have subsided consistent with the direction of paleo-plate motion (Okamura et al., 1992).

The Ogasawara Plateau, Michelson Ridge, and Uda Spur are located at the western tip of the Early Cretaceous Northern Wake
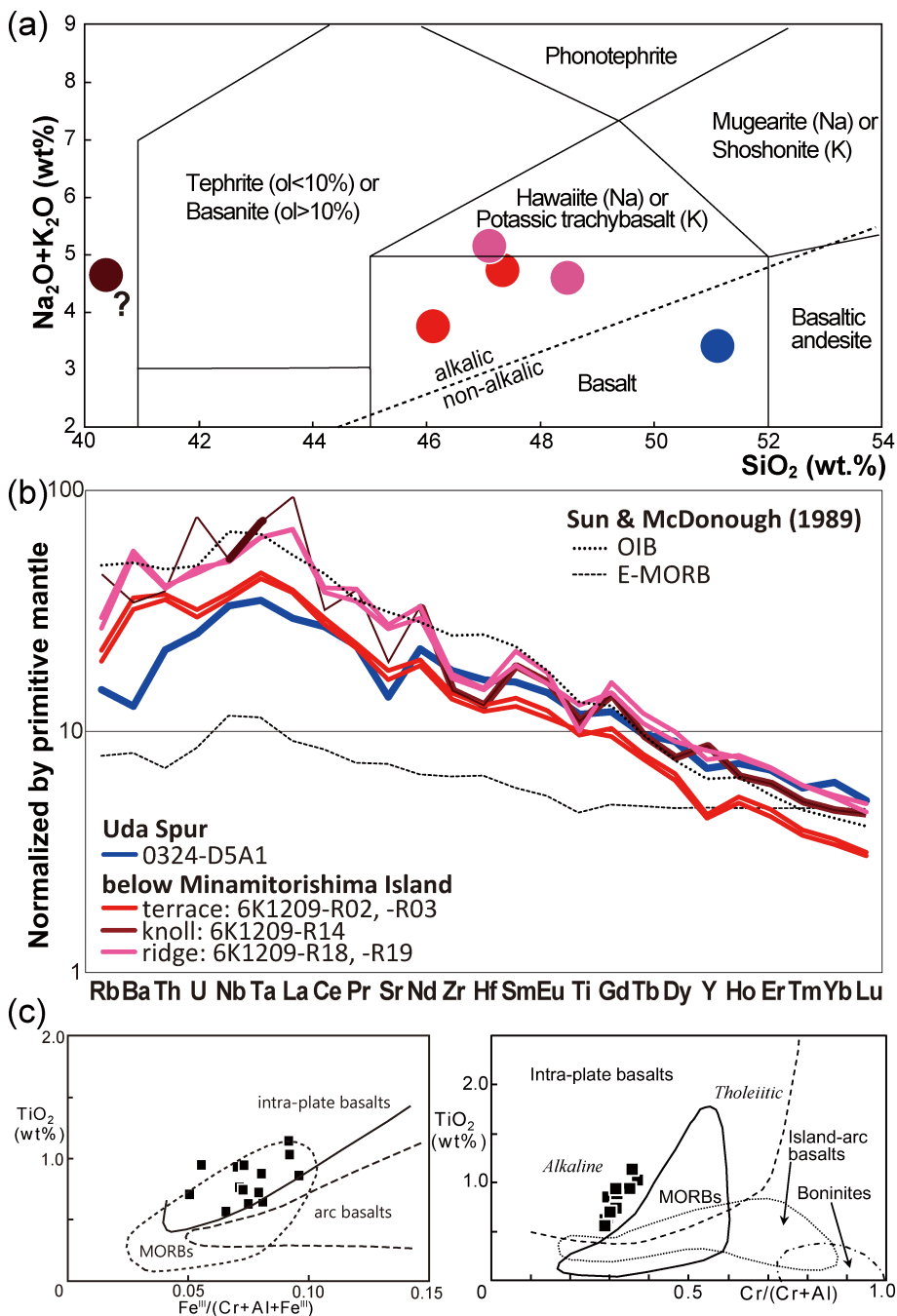
FIGURE 4 Geochemistry of the samples shown as major elements (a) and multi-element variation diagram patterns normalized by 'primitive mantle' (Sun & McDonough, 1989) (b). OIB: ocean island basalt. E-MORB: Enriched mid-ocean ridge basalt. The compositions of samples from submarine slope of Minamitorishima Island showing red (6K1209-R02, -R03), brown (6K1209-R14), and pink (6K1209-R18, -R19). The sample from the Uda Spur (0324D5A1) is shown in blue. Color legends are the same in (a) and (b). Major element compositions of remnant chromian spinels within altered basalts from the Uyeda Ridge (KH87-3 5-003, -006) are shown in (c)

Seamount Chain (Koppers et al., 2003). The basement age obtained for the Uda Spur in this study indicates that this area cannot form part of this seamount chain, as it is significantly younger than the age of the westernmost seamount within the older western part of the Northern Wake Seamount Chain (112.7 ± 0.8 Ma for the Kanrin Guyot; Koppers et al., 2003) (Figure 6).

The fresh glass within sample 0342-D5A1 has a tholeiitic basalt composition (i.e., higher SiO_2 and lower $Na_2O + K_2O$ than OIB) (Table 2) and contains lower concentrations of incompatible elements at a given MgO content than is the case for the other samples analyzed during this study (Figure 4a,b). The Uda Spur extends ~132 km from the central Caster Guyot and is the largest among spurs on the Pacific Plate (e.g., the Umiushi and Fukuro-unagi spurs as well as some

spurs associated with the Hawaii–Emperor seamounts) (Figure 6; Table 4). The formation of spurs from a central edifice reflects higher eruption rates than those associated with other intraplate volcanoes (Smith et al., 2002). The lower concentrations of incompatible elements within this sample combined with the bathymetry of the Uda Spur both reflect higher degree (i.e., tholeiitic) partial melting during the magmatism that formed the spur.

5.2 | Minamitorishima Island

The samples from the northwestern slope of Minamitorishima Island can be divided into two groups, namely dense and vesicular basalts

TABLE 3 Geochemical compositions of chromian spinel in the samples, KH87-3 5-003 and -006

|	KH87-3 D5-003 Chromian spinel								KH87-3 D5-006 Chromian spinel							
SiO_2	0.13	0.13	0.08	0.24	0.17	0.09	0.09	0.12	0.22	0.13	0.16	0.10	0.12	0.16	0.16
TiO_2	0.63	0.62	1.02	1.02	0.55	0.85	1.13	0.92	0.94	0.86	0.75	0.71	0.73	0.93	0.70
Al_2O_3	37.20	37.78	31.79	30.75	38.24	36.11	32.20	34.88	33.28	35.94	36.21	36.55	36.14	36.75	37.76
FeO^*	22.49	21.75	23.79	25.24	20.73	22.97	23.69	22.13	22.35	21.92	21.29	21.64	21.70	22.23	21.01
MnO	0.18	0.15	0.22	0.13	0.17	0.16	0.18	0.18	0.15	0.16	0.20	0.12	0.13	0.16	0.13
MgO	14.26	14.43	13.60	11.98	14.54	14.59	13.55	14.07	12.15	14.79	14.60	14.66	14.30	14.64	13.60
CaO	0.07	0.03	0.00	0.16	0.03	0.02	0.05	0.08	0.10	0.04	0.04	0.03	0.49	0.07	0.13
Na_2O	0.00	0.00	0.01	0.01	0.00	0.00	0.00	0.03	0.00	0.01	0.04	0.01	0.00	0.00	0.05
K_2O	0.01	0.01	0.00	0.02	0.00	0.00	0.01	0.01	0.02	0.00	0.00	0.04	0.03	0.02	0.03
Cr_2O_3	23.11	22.82	27.90	26.95	23.06	22.54	26.65	26.84	26.80	25.00	25.38	23.85	24.91	25.27	24.21
V_2O_3	0.21	0.24	0.29	0.25	0.22	0.26	0.22	0.26	0.25	0.22	0.24	0.18	0.22	0.20	0.26
NiO	0.18	0.25	0.15	0.15	0.19	0.13	0.20	0.12	0.20	0.17	0.10	0.23	0.16	0.17	0.26
P_2O_5	0.00	0.00	0.01	0.00	0.00	0.02	0.00	0.00	0.01	0.00	0.00	0.00	0.29	0.02	0.00
Total	98.45	98.19	98.84	96.91	97.90	97.74	97.97	99.62	96.48	99.24	99.01	98.10	99.22	100.62	98.30
$Mg/(Mg+Fe^{2+})$	0.63	0.64	0.62	0.56	0.64	0.65	0.62	0.63	0.57	0.65	0.64	0.65	0.63	0.64	0.60
$Cr/(Cr+Al)$	0.29	0.29	0.37	0.37	0.29	0.30	0.36	0.34	0.35	0.32	0.32	0.30	0.32	0.32	0.30

Note: FeO^* as total FeO.
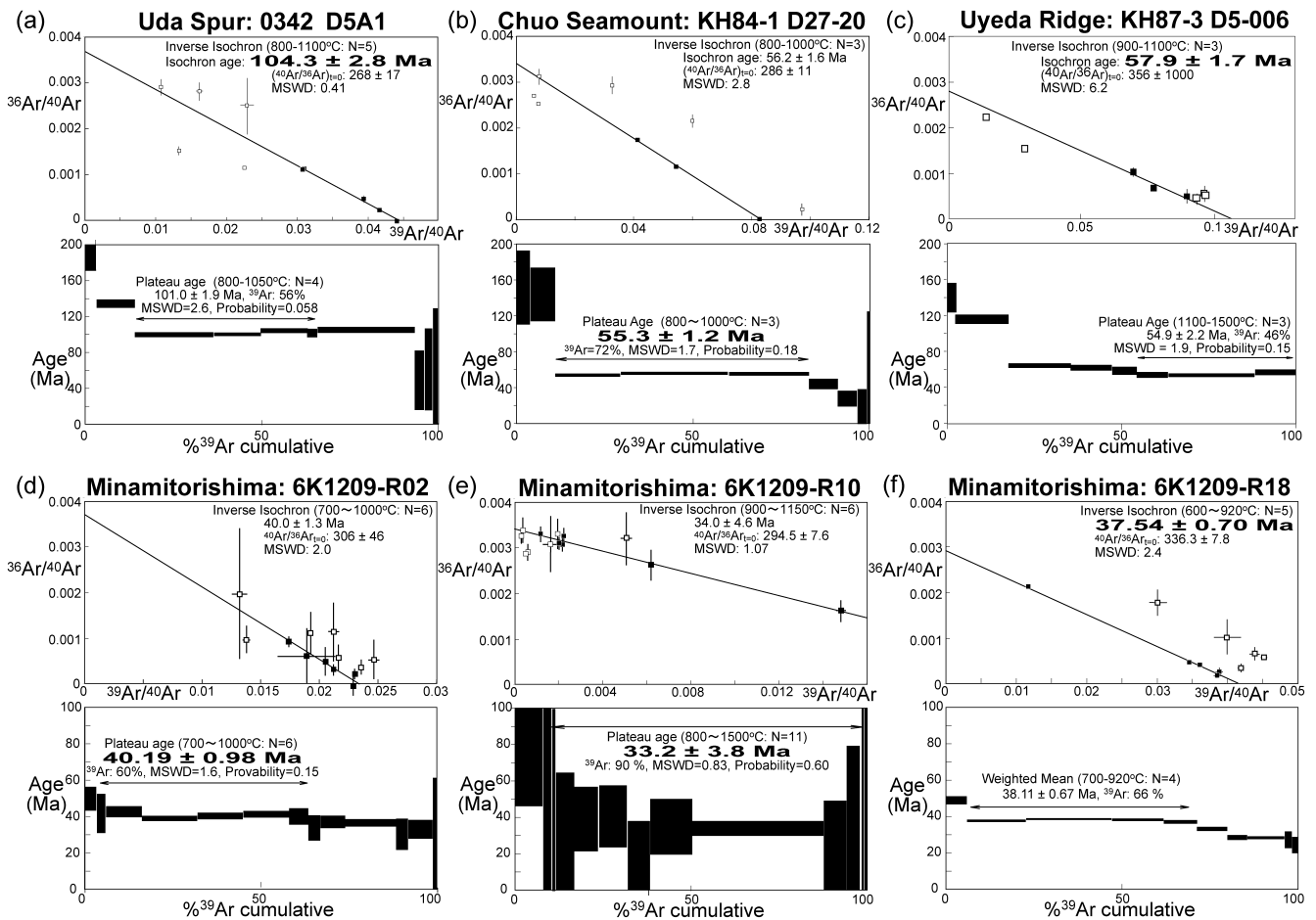
FIGURE 5 Ar–Ar dating results of the six samples (a) to (f). Inverse isochron plots (upper figures) and age spectrums (under figures) are shown for each sample. The preferred ages for each sample are shown within the associated isochron or spectra image. All error bars are shown in 2σ. Error of age results is shown with J-values uncertainties
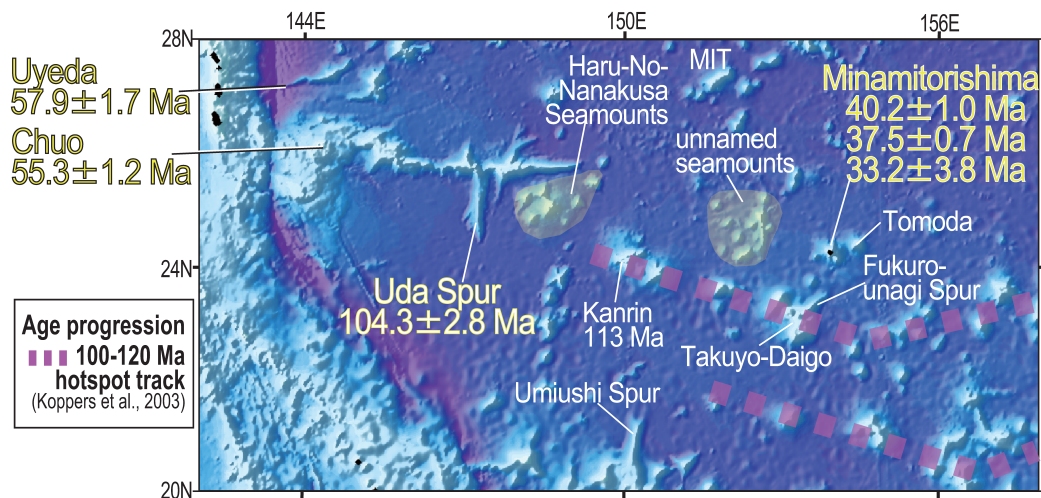
FIGURE 6 Geochronological interpretation of the study area; pink colored dotted lines show the location of previously identified Early Cretaceous hotspot tracks (Koppers et al., 2003)

from the terrace area, and from the ridge and knoll areas, respectively, of this region (Table 1). The latter are grouped together as all of the ridge samples consist of debris or conglomeratic material that is

geochemically, geochronologically, and petrographically similar to the rock types found at the knoll site. Altered sample 6K1209-R14 from the knoll site is only discussed in terms of HFSE concentrations

TABLE 4 Major spurs on the Pacific plate

Spurs	Seamount that the spurs belong to	Length (km)
Uda (this study)	Castor Guyot, Michelson Ridge	132
Eastern tip of Michelson Ridge	Pollux Guyot, Michelson Ridge	119
Fukuro-unagi	Takuyo-Daigo Guyot, Marcus-Wake Seamounts	62
Umiushi	Weiqi and Weiluo Guyots, Magellan Seamounts	85
– (unnamed)	Nintoku Guyot, Emperor Seamount Chain	133
Northern tip of Saint Rogatien Bank	French Frigate Shoals, Hawaiian Ridge	126

given the immobility of these elements during seawater alteration (Philpotts & Hart, 1969; Ludden & Thompson, 1978; Figure 4b). Although both of the dense basalts from the terrace site contain similar concentrations of SiO_2 (45.0–46.6 wt%), their MgO contents (7.6–8.1 wt%) are higher than those of vesicular basalt samples 6K1209-R18 and -R19 (3.8 wt%) (Table 2). The vesicular lavas (samples 6K1209-R14, -R18, and -R19) all have higher incompatible element concentrations than the dense basalts from the terrace area. These vesicular lavas are also depleted in Zr, Hf, and Ti relative to other incompatible elements (Figure 4b).

Dense basalt sample 6K1209-R02 yielded an age of 40.19 ± 0.98 Ma that is significantly older than the ages obtained for the vesicular basalt samples 6K1209-R10 and -R18 (33.2 ± 3.8 and 37.54 ± 0.70 Ma, respectively). This suggests that Minamitorishima Island records two stages of Eocene submarine volcanic eruption that generated pillow lavas and hyaloclastites, respectively (Figure 2). The later volcanic event is similar to those associated with submarine petit-spot volcanos that erupted highly vesicular submarine lavas and hyaloclastites that form small (~1 km diameter) cones typically with a few hundred meters high (Hirano et al., 2006, 2008). The relative Zr, Hf, and Ti depletions in vesicular samples 6K1209-R14, -R18, and -R19 outlined above are also observed both in petit-spot volcanic systems (Hirano et al., 2019; Machida et al., 2015) and the rejuvenated stage lavas after a hiatus following the voluminous shield building stage on hotspot (Bizimis et al., 2013; Clague et al., 2016) (Figure 4b).

The fact that several early Late Cretaceous reefal limestones and a post-Eocene uplift event have been identified in the area around Minamitorishima Island (Aftabuzzaman et al., 2021) means that the Eocene volcanic eruptions identified by ages of 6K1209-R02 and R18 in this study overprinted a previously existing Cretaceous volcanic edifice that might have formed part of the Northern Wake seamount chain defined by Koppers et al. (2003). These volcanic overprints, and later uplift in the area, mean that this island represents a unique part of the northern WPSP because the majority of the Early to middle Cretaceous seamounts within this province became submerged as a result of latest Early to Late Cretaceous sea-level rise (Ocean Drilling Program Leg 144 Shipboard Scientific Party, 1993).

5.3 | Origin of Paleogene overprints

The transition from the main shield building to post-erosional (rejuvenated) evolutionary stages of hotspot-related volcanic edifices lasted 2–3 my on the present-day Hawaiian hotspot (Macdonald & Katsura, 1964), but took more than 10 my on the Early Cretaceous Quesada Seamount within the WPSP (main shield-building to post-shield stages; Hirano et al., 2002). In comparison, this transition was irregular within the Ogasawara Plateau and on Minamitorishima Island, lasting over 50 my until the onset of the Paleogene rejuvenating volcanic event, as the carbonate platforms in these areas formed during erosion after the cessation of the main-shield building stage. This suggests that the Paleogene overprints in the study area may represent the onset of a different magmatic stage that was distinct from the underlying Cretaceous edifice.

Several instances of non-hotspot intraplate volcanism have recently been identified within the Pacific Plate. These include petit-spot alkaline magmatism induced by lithospheric flexure associated with the squeezing-based ascent of magma in the outer rise area of the Japan Trench. This flexure was caused by lithospheric subduction and the coincident production of low volumes of magma from the asthenosphere (Hirano et al., 2006, 2008). These volcanoes have been identified in numerous subduction zone settings elsewhere (e.g., the Tonga, Mariana, and Sunda trenches; Hirano et al., 2008, 2019; Taneja et al., 2016). Although the study area was not located at the front of a trench during the Paleogene, similar volcanism to the petit-spot magmatism outlined above is known to occur in intraplate settings associated with types of tectonic stress, other than subduction (Buchs et al., 2013; Hirano et al., 2016; Uenzelmann-Neben et al., 2012; Valentine & Hirano, 2010). In addition, the deformation of the Pacific Plate, associated with a shift in absolute plate motion, has also been known to generate intraplate volcanism (O'connor et al., 2015). These eruptions involve shallow-sourced tholeiitic rather than OIB-type magmas, contrasted with the alkaline or highly alkaline melts associated with both petit-spot volcanoes and the Paleogene samples analyzed in this study.

An alternative scenario could be that the Paleogene overprints reflect the presence of an unknown age-progression like a hotspot that simply overlapped the known Cretaceous seamounts (Figure 6). As mentioned above, two stages of Paleogene submarine volcanic eruption on the Minamitorishima volcanic edifice in this study plausibly follow the evolutional stages of a hotspot volcano. This scenario is supported by the presence of a geographical lineation that connects the Minamitorishima Island to the Chuo Seamount (284°) and the Uyeda Ridge (289°), and is approximately parallel to the absolute motion of the Pacific Plate since 50 Ma (e.g., as defined by the Hawaiian Ridge and younger Louisville seamount chain; Gripp & Gordon, 2002; Wessel & Kroenke, 2008). This possible age-progressive region of the WPSP could also include the Haru-No-Nanakusa and other unnamed seamounts to the west of Minamitorishima Island and its neighbor Tomoda Seamount (Figure 6). No active hotspots, however, were observed around present Mid-Pacific Mountains where the Paleogene volcanic edifices in this study are back-calculated based on the Pacific absolute

plate motions during Paleogene to present (Wessel & Kroenke, 2008). Further research and sampling of the WPSP are required to better understand the evolution of the seamounts in this region, as well as in the wider western Pacific Plate.

6 | CONCLUSIONS

This study is the first report of Paleogene basaltic rocks of the Western Pacific Seamount Province, an area where only Cretaceous ages have been obtained to date. Samples collected from submarine slopes of Minamitorishima Island yield whole-rock Ar–Ar ages of 40.2 ± 1.0 Ma, 33.2 ± 3.8, and 37.5 ± 0.7 Ma whereas samples from Uyeda Ridge and a knoll on the Chuo Seamount of the Ogasawara Plateau yield ages of 57.9 ± 1.7 and 55.3 ± 1.2 Ma, respectively. Previous research identified Upper Cretaceous limestones and fossils from the Chuo Seamount and the Minamitorishima Island (Aftabuzzaman et al., 2021; Konishi, 1985; Shiba, 1979), indicating that these Paleogene basalts reflect an overprinting volcanic event, or vents that affected existing Cretaceous volcanic edifices. A mid-Cretaceous age of 104.3 ± 2.8 Ma was also obtained for the Uda Spur, which extends south from the Michelson Ridge and the connected Ogasawara Plateau. This age may therefore reflect the age of a basement edifice along the Ogasawara Plateau and related ridges (i.e., the Michelson Ridge and Uda Spur) as the limestone platforms along the Ogasawara Plateau and the Michelson Ridge formed at 110–80 Ma. The timing of formation of the Uda Spur is, however, not associated with the formation of a western extension to the Early Cretaceous Northern Wake seamount chain.

ORCID

Naoto Hirano https://orcid.org/0000-0003-0980-3929
Hirochika Sumino https://orcid.org/0000-0002-4689-6231
Taisei Morishita https://orcid.org/0000-0003-2604-6640
Shiki Machida https://orcid.org/0000-0002-1069-7214
Kazutaka Yasukawa https://orcid.org/0000-0002-3216-8698
Takafumi Hirata https://orcid.org/0000-0003-4683-9103
Yasuhiro Kato https://orcid.org/0000-0002-5711-8304

REFERENCES

Aftabuzzaman, M. R., Yomogoda, K., Suzuki, S., Takayanagi, H., Ishigaki, A., Machida, S., Asahara, Y., Yamamoto, K., Hirano, N., Sano, S., Chiyonobu, S., Bassi, D., & Iryu, Y. (2021). Carbonate rocks off Minami-Tori-Shima and their depositional history. *Island Arc* (submitted in this issue).

Bizimis, M., Salters, V. J. M., Garcia, M. O., & Norman, M. D. (2013). The composition and distribution of the rejuvenated component across the Hawaiian plume: Hf-Nd-Sr-Pb isotope systematics of Kaula lavas and pyroxenite xenoliths. *Geochemistry, Geophysics, Geosystems, 14,* 4458–4478.

Buchs, D. M., Pilet, S., Cosca, M., Flores, K. E., Bandini, A. N., & Baumgartner, P. O. (2013). Low-volume intraplate volcanism in the Early/Middle Jurassic Pacific basin documented by accreted sequences in Costa Rica. *Geochemistry, Geophysics, Geosystems, 14,* 1552–1568.

Clague, D. A., Frey, F. A., Garcia, M. O., Huang, S., McWilliams, M., & Beeson, M. H. (2016). Compositional heterogeneity of the Sugarloaf melilite nephelinite flow, Honolulu Volcanics, Hawai'i. *Geochimica et Cosmochimica Acta, 185,* 251–277.

Davis, A. S., Gray, L. B., Clague, D. A., & Hein, J. R. (2002). The Line Islands revisited: New $^{40}Ar/^{39}Ar$ geochronologic evidence for episodes of volcanism due to lithospheric extension. *Geochemistry, Geophysics, Geosystems, 3*(3), 1–28. https://doi.org/10.1029/2001GC000190

Duncan, R. A., & Clague, D. A. (1985). Pacific Plate motion recorded by liner volcanic chains. In A. E. M. Narin, F. G. Stehli, & S. Uyeda (Eds.), *The ocean basins and margins: The Pacific ocean* (Vol. 7A, pp. 89–121). Plenum.

Flish, M. (1982). Potassium-argon analysis. In G. S. Odin (Ed.), *Numerical dating in stratigraphy* (pp. 151–158). Wiley.

Geldmacher, J., Hoernle, K., Bogaard, P., Zankl, G., & Garbe-Schönberg, D. (2001). Earlier history of the ≥70-Ma-old Canary hotspot based on the temporal and geochemical evolution of the Selvagen Archipelago and neighboring seamounts in the eastern North Atlantic. *Journal of Volcanology and Geothermal Research, 111*(1–4), 55–87.

Gripp, A. E., & Gordon, R. G. (2002). Young tracks of hotspots and current plate velocities. *Geophysical Journal International, 150,* 321–361.

Handschumacher, D. W., Sager, W. W., Hilde, T. W. C., & Bracey, D. R. (1988). Pre-Cretaceous tectonic evolution of the Pacific plate and extension of the geomagnetic polarity reversal time scale with implications for the origin of the Jurassic "Quiet Zone". *Tectonophysics, 155,* 365–380.

Hardebeck, J., & Anderson, D. L. (1996). Eustasy as a test of a Cretaceous superplume hypothesis. *Earth and Planetary Science Letters, 137,* 101–108.

Henderson, L. J., Gordon, R. G., & Engebretson, D. C. (1984). Mesozoic aseismic ridges on the Frallaon Plate and southward migration of shallow subduction during the Laramide orogeny. *Tectonics, 3*(2), 121–132.

Hess, J. C., & Lippolt, H. J. (1994). Compilation of K-Ar measurements on HD-B1 standard biotite; 1994 status report. In G. S. Odin (Ed.), *Bulletin of liaison and informations, IUGS subcommission on geochronology (International Commission on Stratigraphy), Phanerozoic time scale* (Vol. 12, pp. 19–23).

Hirano, N., Koppers, A. A. P., Takahashi, A., Fujiwara, T., & Nakanishi, M. (2008). Seamounts, knolls and petit spot monogenetic volcanoes on the subducting Pacific Plate. *Basin Research, 20,* 543–553.

Hirano, N., Machida, S., Sumino, H., Shimizu, K., Tamura, A., Morishita, T., Iwano, H., Sakata, S., Ishii, T., Arai, S., Yoneda, S., Danhara, T., & Hirata, T. (2019). Petit-spot volcanoes on the oldest portion of the Pacific Plate. *Deep-Sea Research Part I, 154,* 103142.

Hirano, N., Nakanishi, M., Abe, N., & Machida, S. (2016). Submarine lava fields in French Polynesia. *Marine Geology*, *373*, 39–48.

Hirano, N., Ogawa, Y., & Saito, K. (2002). Long-lived early cretaceous seamount volcanism in the Mariana Trench, Western Pacific Ocean. *Marine Geology*, *189*, 371–379.

Hirano, N., Takahashi, E., Yamamoto, J., Abe, N., Ingle, S. P., Kaneoka, I., Kimura, J. –. I., Hirata, T., Ishii, T., Ogawa, Y., Machida, S., & Suyehiro, K. (2006). Volcanism in response to plate flexure. *Science*, *313*, 1426–1428.

Imai, N., Terashima, S., Itoh, S., & Ando, A. (1995). 1994 compilation of analytical data for minor and trace elements in seventeen GSJ geochemical reference samples 'Igneous Rock Series'. *Geostandards Newsletter*, *19*, 135–213.

Iwata, N. (1998). *Geochronological study of the Deccan volcanism by the $^{40}Ar–^{39}Ar$ method* (Doctor Thesis), University of Tokyo, pp. 168.

Jackson, M. G., Halldórsson, S. A., Price, A., Kurz, M. D., Konter, J. G., Koppers, A. A. P., & Day, J. M. D. (2020). Contrasting old and young volcanism from Aitutaki, Cook Islands: Implications for the origins of the Cook-Austral volcanic chain. *Journal of Petrology*, *61*, egaa037. https://doi.org/10.1093/petrology/egaa037

Kasuga, S., Shimotori, F., & Members of Continental Surveys Office. (1995). Geomorphology and tectonics of the Ogasawara Plateau and its surrounding area in the north Pacific basin. *Report of Hydrographic and Oceanographic Researches, Japan Coast Guard*, *31*, 23–44 (in Japanese with English abstract).

Kato, Y., Fujinaga, K., Nakamura, K., Takaya, Y., Kitamura, K., Ohta, J., Toda, R., Nakashima, T., & Iwamori, H. (2011). Deep-sea mud in the Pacific Ocean as a potential resource for rare-earth elements. *Nature Geoscience*, *4*, 535–539.

Kato, Y., Fujinaga, K., & Suzuki, K. (2005). Major and trace element geochemistry and Os isotopic composition of metalliferous umbers from the Late Cretaceous Japanese accretionary complex. *Geochemistry, Geophysics, Geosystems*, *6*, Q07004.

Konishi, K. (1985). Cretaceous reefal fossils dredged from two seamounts of the Ogasawara Plateau. In K. Kobayashi (Ed.), *Preliminary report of the Hakuho Maru cruise KH84-1* (pp. 169–180). Ocean Research Institute, The University of Tokyo.

Koppers, A. A. P., Staudigel, H., Pringle, M. S., & Wijbrans, J. R. (2003). Short-lived and discontinuous intraplate volcanism in the south Pacific: Hot spots or extensional volcanism? *Geochemistry, Geophysics, Geosystems*, *4*, 1089. https://doi.org/10.1029/2003gc000533

Koppers, A. A. P., Staudigel, H., & Wijbrans, J. R. (2000). Dating crystalline groundmass separates of altered Cretaceous seamount basalts by the $^{40}Ar/^{39}Ar$ incremental heating technique. *Chemical Geology*, *166*, 139–158.

Koppers, A. A. P., Staudigel, H., Wijbrans, J. R., & Pringle, M. S. (1998). The Magellan seamount trail; implications for Cretaceous hotspot volcanism and absolute Pacific Plate motion. *Earth and Planetary Science Letters*, *163*, 53–68.

Larson, R. L. (1991). Geological consequences of superplumes. *Geology*, *19*, 963–966.

Ludden, J. N., & Thompson, G. (1978). Behaviour of rare earth elements during submarine weathering of tholeiitic basalt. *Nature*, *274*, 147–149.

Macdonald, G. A., & Katsura, T. (1964). Chemical composition of Hawaiian lavas. *Journal of Petrology*, *5*, 82–133.

Machida, S., Hirano, N., Sumino, H., Hirata, T., Yoneda, S., & Kato, Y. (2015). Petit-spot geology reveals melts in upper-most asthenosphere dragged by lithosphere. *Earth and Planetary Science Letters*, *426*, 267–279.

Machida, S., Ishii, T., Kimura, J. –. I., Awaji, S., & Kato, Y. (2008). Petrology and geochemistry of cross-chains in the Izu-Bonin back arc: Three mantle components with contributions of hydrous liquids from a deeply subducted slab. *Geochemistry, Geophysics, Geosystems*, *9*, 1–31.

Martin, U., Breitkreuz, C., Egenhoff, S., Enos, P., & Jansa, L. (2004). Shallow-marine phreatomagmatic eruptions through a semi-solidified carbonate platform (ODP Leg 144, Site 878, Early Cretaceous, MIT Guyot, West Pacific). *Marine Geology*, *204*, 251–272.

Nagaoka, S., Uchida, M., Kasuga, S., Kaneko, Y., Kato, Y., Kawai, K., & Seta, H. (1989). Tectonics of the Ogasawara Plateau in the western Pacific Ocean. *Report of Hydrographic and Oceanographic Researches, Japan Coast Guard*, *25*, 23–91 (in Japanese with English abstract).

Norman, M. D., Griffin, W. L., Pearson, N. J., Garcia, M. O., & O'Reilly, S. Y. (1998). Quantitative analysis of trace element abundances in glasses and minerals: A comparison of laser ablation inductively coupled plasma mass spectrometry, solution inductively coupled plasma mass spectrometry, proton microprobe and electron microprobe data. *Journal of Analytical Atomic Spectrometry*, *13*, 477–482.

O'connor, J. M., Hoernle, K., Müller, R. D., Morgan, J. P., Butterworth, N. P., Hauff, F., Sandwell, D. T., Jokat, W., Wijbrans, J. R., & Stoffers, P. (2015). Deformation-related volcanism in the Pacific Ocean linked to the Hawaiian–Emperor bend. *Nature Geoscience*, *8*, 393–397.

Ocean Drilling Program Leg 144 Shipboard Scientific Party. (1993). Insight on the formation of Pacific guyots from ODP Leg 144. *Eos*, *74*, 358–359.

Ohara, Y., Kato, Y., Yoshida, T., & Nishimura, A. (2015). Geoscientific characteristics of the seafloor of the southern ocean of Japan revealed by Japan's continental shelf survey. *Journal of Geography (Chigaku Zasshi)*, *124*, 687–709 (in Japanese with English Abstract).

Oikawa, M., & Morishita, T. (2009). Submarine topography in the east sea to the Minami-Tori Shima Island, North West Pacific Ocean. *Report of Hydrographic and Oceanographic Researches*, *45*, 13–22 (in Japanese with English Abstract).

Okamura, Y., Murakami, F., Kishimoto, K., & Saito, E. (1992). Seismic profiling survey of the Ogasawara Plateau and the Michelson Ridge, western Pacific: Evolution of Cretaceous guyots and deformation of a subducting oceanic plateau. *Bulletin of the Geological Survey of Japan*, *43*, 237–256.

Philpotts, J. A., & Hart, S. S. R. (1969). Submarine basalts: Some K, Rb, Sr, Ba, rare-earth, H_2O, and CO_2 data bearing on their alteration, modification by plagioclase, and possible source materials. *Earth and Planetary Science Letters*, *7*, 293–299.

Sager, W. W., Duncan, R. A., & Handschumacher, D. W. (1993). *Paleomagnetism of the Japanese and Marcus-Wake Seamounts, Western Pacific Ocean*. *Geophysical Monograph Series* (Vol. 77, pp. 401–435). AGU.

Shiba, M. (1979). Geological history of the Yabe guyot to the east of the Ogasawara Islands. *Journal of Geological Society of Japan*, *85*, 209–220 (in Japanese with English abstract).

Smith, D. K., Kong, L. S. L., Johnson, K. T., & Reynolds, J. R. (2002). *Volcanic morphology of the submarine Puna Ridge, Kilauea volcano*. *Geophysical Monograph Series* (Vol. 128, pp. 125–142).

Smoot, N. C. (1983). Multi-beam surveys of the Michelson Ridge guyots: Subduction or obduction. *Tectonophysics*, *99*, 363–380.

Smoot, N. C., & Heffner, J. H. (1986). Bathymetry and possible tectonic interaction of the Uyeda Ridge with its environment. *Tectonophysics*, *124*, 23–36.

Sun, S.-S., & McDonough, W. F. (1989). Chemical and isotopic systematics of oceanic basalts: Implications for mantle composition and processes. *Geological Society, London, Special Publications*, *42*, 313–345.

Takayanagi, H., Iryu, Y., Yamada, T., Oda, M., Yamamoto, K., Sato, T., Chiyonobu, S., Nishimura, A., Nakazawa, T., & Shiokawa, S. (2007). Carbonate deposits on submerged seamounts in the northwestern Pacific Ocean. *Island Arc*, *16*, 394–419.

Taneja, R., Rushmer, T., Blichert-Toft, J., Turner, S., & O'Neill, C. (2016). Mantle heterogeneities beneath the Northeast Indian Ocean as sampled by intra-plate volcanism at Christmas Island. *Lithos*, *262*, 561–575.

Uenzelmann-Neben, G., Schmidt, D. N., Niessen, F., & Stein, R. (2012). Intraplate volcanism off South Greenland: Caused by glacial rebound? *Geophysical Journal International, 190*, 1–7.

Valentine, G. A., & Hirano, N. (2010). Mechanisms of low-flux intraplate volcanic fields—Basin and Range (North America) and northwest Pacific Ocean. *Geology, 38*, 55–58.

Wessel, P., & Kroenke, L., W. (2008) Pacific absolute plate motion since 145 Ma: An assessment of the fixed hot spot hypothesis. *Journal of Geophysical Research, 113* (B6), B06101.

Winterer, L. E., Natland, J. H., & Waasbergen, R. J. V. (1993). *Cretaceous guyots in the northwest Pacific: An overview of their geology and geophysics. Geophysical Monograph Series* (Vol. 77, pp. 307–334). AGU.

SUPPORTING INFORMATION

Additional supporting information may be found online in the Supporting Information section at the end of this article.